Palaeogeography, Palaeoclimatology, Palaeoecology 333–334 (2012) 1–12

Contents lists available at SciVerse ScienceDirect

Palaeogeography, Palaeoclimatology, Palaeoecology

journal homepage: www.elsevier.com/locate/palaeo

New constraints on climate forcing and variability in the circum-Mediterranean region from magnetic and geochemical observations of sapropels S1, S5 and S6

Qingsong Liu [a,*], Juan C. Larrasoaña [b], José Torrent [c], Andrew P. Roberts [d,1], Eelco J. Rohling [d], Zhifeng Liu [a], Zhaoxia Jiang [a]

[a] Paleomagnetism and Geochronology Laboratory (SKL-LE), Institute of Geology and Geophysics, Chinese Academy of Sciences, Beijing 100029, People's Republic of China
[b] Instituto Geológico y Minero de España, Unidad de Zaragoza, C/Manuel Lasala 44, 9°B, 50006 Zaragoza, Spain
[c] Departamento de Agronomía, Universidad de Córdoba, Edificio C4, Campus de Rabanales, 14071 Córdoba, Spain
[d] School of Ocean and Earth Science, University of Southampton, European Way, National Oceanography Centre, Southampton, SO14 3ZH, UK

ARTICLE INFO

Article history:
Received 28 June 2011
Received in revised form 24 February 2012
Accepted 26 February 2012
Available online 10 March 2012

Keywords:
Sapropels
Circum-Mediterranean region
Environmental change
Savannah landscapes

ABSTRACT

Eastern Mediterranean sapropels are organic-rich layers whose formation was triggered during boreal summer insolation maxima (precession minima). Sapropel formation is associated with increased precipitation and run-off from Europe and North Africa, although the relative influence of high- and low-latitude climate mechanisms is not fully resolved. Likewise, it remains uncertain how centennial-scale interruptions in conditions that give rise to sapropels may reflect atmospheric circulation changes in low latitudes. We present magnetic, geochemical, and diffuse reflectance spectroscopy data from three sapropels that are representative of glacial (S6) and interglacial (S1, S5) conditions in the eastern Mediterranean Sea to assess environmental changes associated with sapropel formation. The extent of diagenetic magnetite dissolution and authigenic formation of fine-grained greigite in these sapropels and their underlying dissolution intervals are linked to enhanced sulphidic conditions during sapropel formation. Aeolian hematite and goethite are largely unaffected by this reductive dissolution except within the interglacial sapropel S5 and its underlying dissolution interval, which formed under relatively stronger sulphidic conditions. Nevertheless, low hematite contents indicate that the three studied sapropels accumulated under reduced aeolian dust inputs in response to an intensified African monsoon, which resulted in expansion of savannah landscapes into NE Saharan dust source areas. Small variations in goethite contents across sapropels indicate additional aeolian entrainment of goethite that formed under previous wet phases in the NE Sahara or in subtropical savannahs located further south. We link short-lived dust abundance peaks within sapropels S1 and S6 to centennial-scale periods of enhanced bottom-water circulation reported previously for these sapropels. Although these sapropel interruptions are driven by high-latitude cooling events, our results indicate that such centennial-scale episodes of atmospheric reorganization affected not only the eastern Mediterranean northern borderlands, but also subtropical North Africa. Overall, our results point to a dominant low-latitude forcing on sapropel formation via boreal summer insolation maxima and intensification of the African monsoon.

1. Introduction

Eastern Mediterranean sapropels are organic-rich, dark-coloured layers that are cyclically intercalated with organic-poor sediments and that have been deposited from the Late Miocene to Holocene (Hilgen, 1991; Rohling, 1994; Lourens et al., 1996; Schenau et al., 1999; Emeis et al., 2000; Köhler et al., 2008). Sapropel formation was triggered by periodic (ca 22 kyr) changes in solar energy received in the northern tropics and mid-latitudes during summer insolation maxima, which corresponds to precession minima (Hilgen, 1991; Lourens et al., 1996; Emeis et al., 2000). During periods of sapropel formation, intensification (Rossignol-Strick, 1983; Lourens et al., 2001; Rohling et al., 2004) and enhanced northward penetration (Rohling et al., 2002a; Larrasoaña et al., 2003a) of the African monsoon, coupled with wetter conditions in Europe (Rohling and Hilgen, 1991; Tuenter et al., 2003; Kotthoff et al., 2008), led to increased freshwater discharge into the eastern Mediterranean along both the north African and eastern European margins. Tzedakis (2007, 2009) argued that pollen data may suggest the persistence of considerable summer aridity in the European. Whether from the monsoon alone, or from the monsoon and from European margins, however, the freshwater input resulted in a surface water buoyancy increase, which led in turn to deterioration of deep-water ventilation (see Rohling, 1994 for an overview). In any case, the episodes of reduced deep-water ventilation appear to have coincided with

* Corresponding author.
E-mail addresses: qsliu@mail.iggcas.ac.cn, liux0272@yahoo.com (Q. Liu).
[1] Now at: Research School of Earth Sciences, The Australian National University, Canberra, ACT 0200, Australia.

0031-0182/$ – see front matter © 2012 Elsevier B.V. All rights reserved.
doi:10.1016/j.palaeo.2012.02.036

enhanced export productivity to the sea floor (Rohling and Gieskes, 1989; Thomson et al., 1995, 1999), which favoured production and preservation of organic matter in basins typically deeper than ~300 m (Rohling and Gieskes, 1989; Rohling et al., 2006). Periods of sapropel formation also coincided with a marked decrease in airborne dust input (Calvert and Fontugne, 2001; Lourens et al., 2001; Larrasoaña et al., 2003a) from the savannah-covered Sahara desert (Krom et al., 1999; Wehausen and Brumsack, 2000; Weldeab et al., 2002; Larrasoaña et al., 2003a). High-resolution studies have shown that periods of decreased bottom water ventilation at times of sapropel formation were episodically interrupted during periods of increased northerly winter air incursions from continental Europe (Rohling et al., 1997, 2002a; Mercone et al., 2000; Casford et al., 2003). It remains to be established whether these centennial-scale periods were also characterized by significant changes in atmospheric circulation at the low latitudes.

Here we present a detailed rock magnetic, geochemical and diffuse reflectance spectroscopy (DRS) dataset for three distinctive sapropels that typify the range of paleoclimatic and paleoceanographic conditions that prevailed in the eastern Mediterranean during periods of sapropel formation since the intensification of the northern hemisphere glaciation at around 0.9 Ma (Emeis et al., 2000). Sapropels S1 and S5 accumulated at the beginning of the current interglacial (~6–10 kyr BP; marine isotopic stage MIS 1; insolation cycle Si2; Langereis et al., 1997; Emeis et al., 2000; Mercone et al., 2000) and during the last interglacial (~124 kyr BP; MIS 5e; Si12; Langereis et al., 1997; Emeis et al., 2000; Rohling et al., 2002a, 2004, 2006; Osborne et al., 2008, 2010), respectively. Sapropel S6 accumulated during a glacial period (~172 kyr BP; MIS 6; Si16; Langereis et al., 1997; Emeis et al., 2000; Calvert and Fontugne, 2001; Casford et al., 2003). By studying sapropels that accumulated during both glacial and interglacial periods and that were linked to tropical summer insolation peaks of different amplitudes, we aim to elucidate the role of high-latitude (glacial–interglacial variability) versus low-latitude (tropical insolation) mechanisms that drive sapropel formation.

Geochemical data have been used to infer paleoclimatic and paleoceanographic scenarios during periods of sapropel formation. For example, Ba/Al ratios have been used to indicate variations in organic carbon flux to the seafloor, and therefore to provide a proxy for productivity (Pruysers et al., 1993; Thomson et al., 1995, 1999; Wehausen and Brumsack, 2000; Calvert and Fontugne, 2001; Mercone et al., 2001). Ti/Al ratios have been used to distinguish the relative contributions of riverine supply and Saharan aeolian dust (Wehausen and Brumsack, 2000; Calvert and Fontugne, 2001; Lourens et al., 2001). V/Al ratios have been used to indicate bottom water oxygen contents and hence the strength of bottom water ventilation (Calvert and Fontugne, 2001). Fe/Al and Ni/Al ratios have been used to determine the strength of sulphate-reducing (i.e. sulphidic) conditions and to identify diagenetic mobilization of these redox sensitive elements that result from degradation of organic matter in sapropels (Thomson et al., 1995; van Santvoort et al., 1997; Warning and Brumsack, 2000; Calvert and Fontugne, 2001).

Magnetic properties provide complementary information on the paleoclimatic and paleoceanographic scenarios during periods of sapropel formation. The anhysteretic remanent magnetization (ARM) has been used to detect changes in magnetite contents in sapropels and their underlying sediments. The concentration of magnetite in these sediments is governed by the strength of reductive dissolution, which is in turn linked to the strength of sulphidic conditions during sapropel formation. Since the latter depends on the interplay between the amount of organic carbon reaching the sediment and the oxygen content of the bottom waters, the ARM can provide additional information on these two paleoceanographic variables (Langereis et al., 1997; van Santvoort et al., 1997; Roberts et al., 1999, 2010; Kruiver and Passier, 2001; Passier et al., 2001; Passier and Dekkers, 2002; Larrasoaña et al., 2003b, 2006). The magnetic parameter κ_{fd}%, which is based on measurement of the magnetic susceptibility at different frequencies, can provide insights into the concentration of ultrafine superparamagnetic (SP) particles that occur within a narrow grain size range (~15–25 nm) (Oldfield et al., 1985; Dearing et al., 1996), that is linked to the strength of sulphidic conditions in sapropels. Alternating field (AF) demagnetization at 150 milliTesla (mT) of an isothermal remanent magnetization imparted at 1 T (labelled $IRM_{AF@150\ mT}$; see Larrasoaña et al., 2003a, 2006) helps to portray variations in the supply of hematite-rich aeolian dust derived from the Sahara desert and, hence, paleoclimate variations in north Africa in response to monsoon dynamics. $IRM_{AF@150\ mT}$ represents an improvement with respect to Ti/Al ratios because it provides information on absolute dust contents instead of relative variations between aeolian and fluvial terrigenous sources (Larrasoaña et al., 2003a).

In addition to such parameters, we here use DRS data to estimate total concentrations of aeolian hematite and goethite (Balsam et al., 1995; Torrent et al., 2007). This is important because goethite is likely to fingerprint different paleoclimatic conditions in the source area (Maher, 1986; Balsam et al., 1995) and its occurrence has remained elusive to standard rock magnetic techniques (Heslop et al., 2007). A comparison of proxies for aeolian dust and riverine supply with goethite (Heslop et al., 2007) and hematite (Heslop et al., 2007; Larrasoaña et al., 2008) abundances further demonstrate the link between these two minerals with the supply of Saharan dust and not to riverine supply.

Previous combined rock magnetic and geochemical studies of sapropels have been based on data measured at lower resolutions (e.g., van Santvoort et al., 1997; Köhler et al., 2008), on data from u-channel samples (e.g., Larrasoaña et al., 2003a, 2003b, 2006, 2008) whose resolution is limited by the ~4 cm-wide magnetometer response function (Roberts, 2006), or on much higher resolution studies of S1 only where magnetic and geochemical data were not reported from its observed interruption intervals (Kruiver and Passier, 2001; Passier et al., 2001; Passier and Dekkers, 2002; Garming et al., 2004). Our study has been conducted at sufficiently high resolution to detect interruptions and provides insights into the underlying mechanisms that drive sapropel formation, and of the paleoclimatic significance of these short-lived interruptions of sapropels that accumulated under distinctive paleoclimatic scenarios.

2. Sampling and experiments

Discrete samples were collected (using standard 8 cm^3 paleomagnetic cubes) back-to-back across the three selected sapropels (S1, S5, and S6) and their surrounding sediments from Ocean Drilling Program (ODP) Hole 967C, which was recovered on the northern slope of Erathostenes Seamount at a water depth of 2553 m (Shipboard Scientific Party, 1996) (Fig. 1). Samples were collected over stratigraphic intervals of 0.65 m and 2.08 m through sapropels S1 and S5–S6, respectively. The visual expressions (dark colouration) of sapropels S1, S5 and S6 are about 20, 29 and 39 cm thick in this core, respectively. They have frequent mm- to cm-thick laminations, which are occasionally burrowed at their tops, and contain no visible evidence for interruption by organic-poor sediments (Shipboard Scientific Party, 1996; Emeis et al., 2000) (Figs. 2 and 3). These sapropels are interbedded between grey and yellowish brown clayey nannofossil oozes that are often bioturbated. Some 0.50 m above S6, a 10-cm-thick ash-rich turbidite is found. Available geochemical data for S5 indicate a maximum total organic carbon (TOC) content of 4.3 wt.%, with values >2% throughout the whole sapropel (Emeis et al., 1998). Lower resolution data from neighbouring Hole 967A indicate comparable TOC values of 4.27 wt.% for S6, and lower TOC values of 2.38 wt.% for S1 (Shipboard Scientific Party, 1996). Based on the age of S6 (172 ka; Emeis et al., 2000) and the stratigraphic thickness above it, a mean accumulation rate of 5.2 cm/kyr for the studied sapropels and surrounding sediments can be inferred (Emeis et al., 2000).

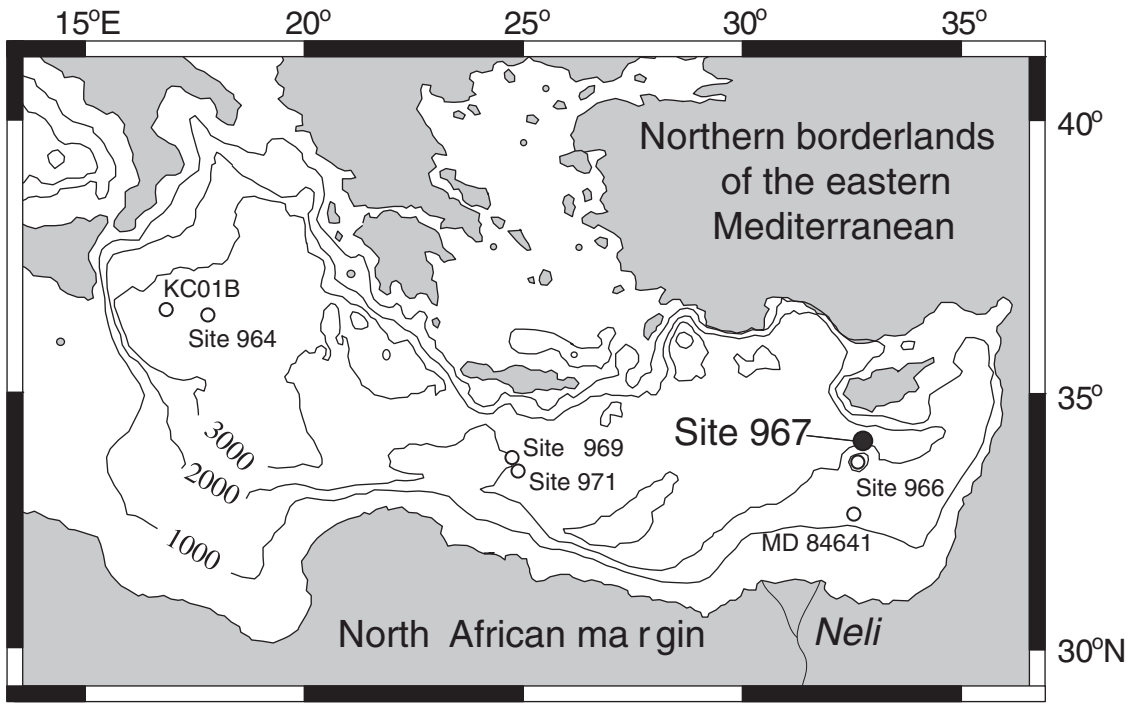

Fig. 1. Map of the eastern Mediterranean Sea with location of the studied site (ODP Site 967) in bold and of other cores mentioned in the manuscript (open circles). NAM and NBEM stand for north African margin and northern borderlands of the Eastern Mediterranean, respectively.

For each collected sample, low-field magnetic susceptibility (κ) was measured at frequencies of 470 (κ_{lf}) and 4700 Hz (κ_{hf}) using a Bartington Instruments MS-2 magnetic susceptibility meter. κ_{fd}% is defined as $((\kappa_{lf}-\kappa_{hf})/\kappa_{lf})\times 100\%$, where κ_{lf} and κ_{hf} are κ values measured at low- and high-frequency, respectively. An ARM was imparted using an AF of 150 mT and a superimposed 50 μT direct current bias

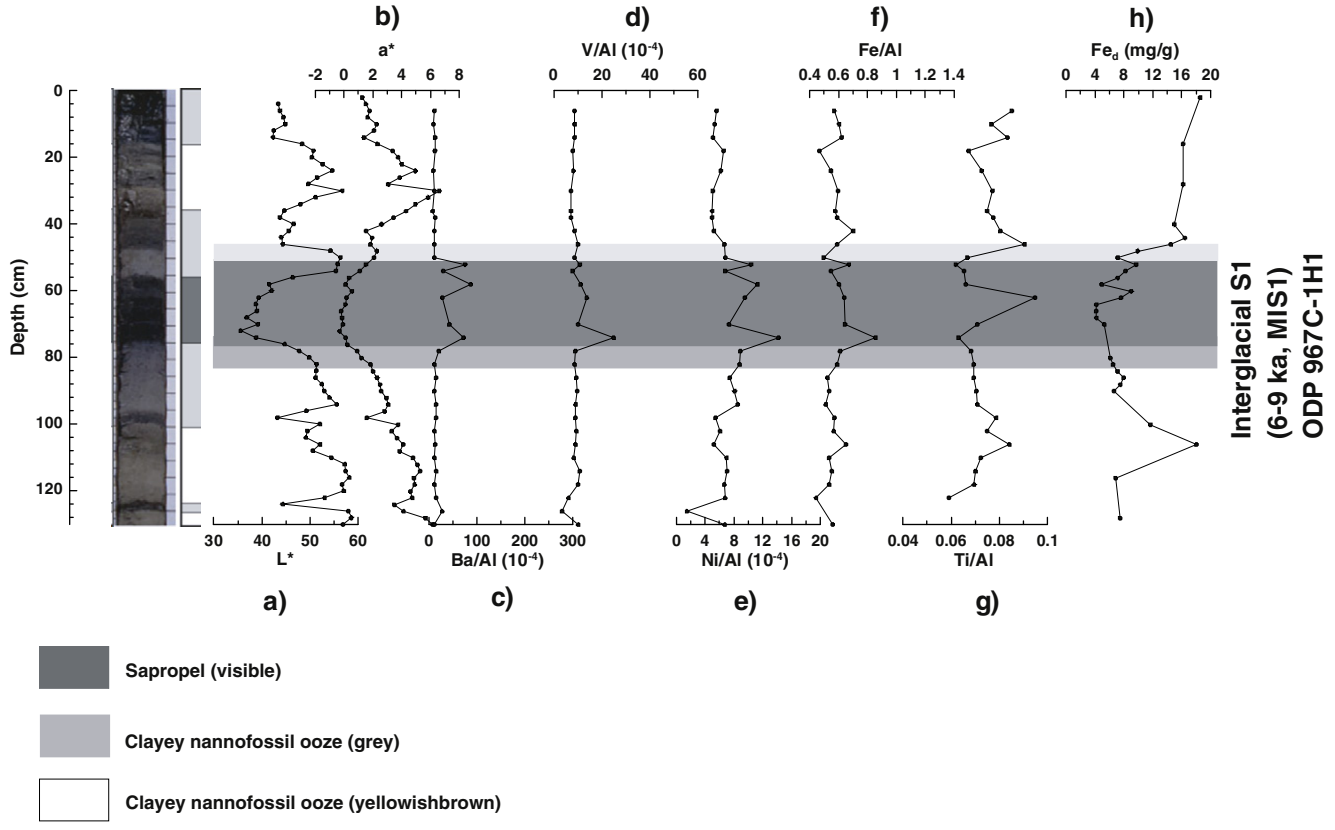

Fig. 2. Stratigraphic log and variations in colour indices (L* and a*) and geochemical parameters for sapropel S1. The dark grey bar indicates the visible portion of the sapropel. The lighter grey bars above and below the sapropel indicate the positions of oxidation and dissolution intervals, respectively. The same scales are used on corresponding axes of graphs in successive figures to enable direct comparison of results from different sapropels.

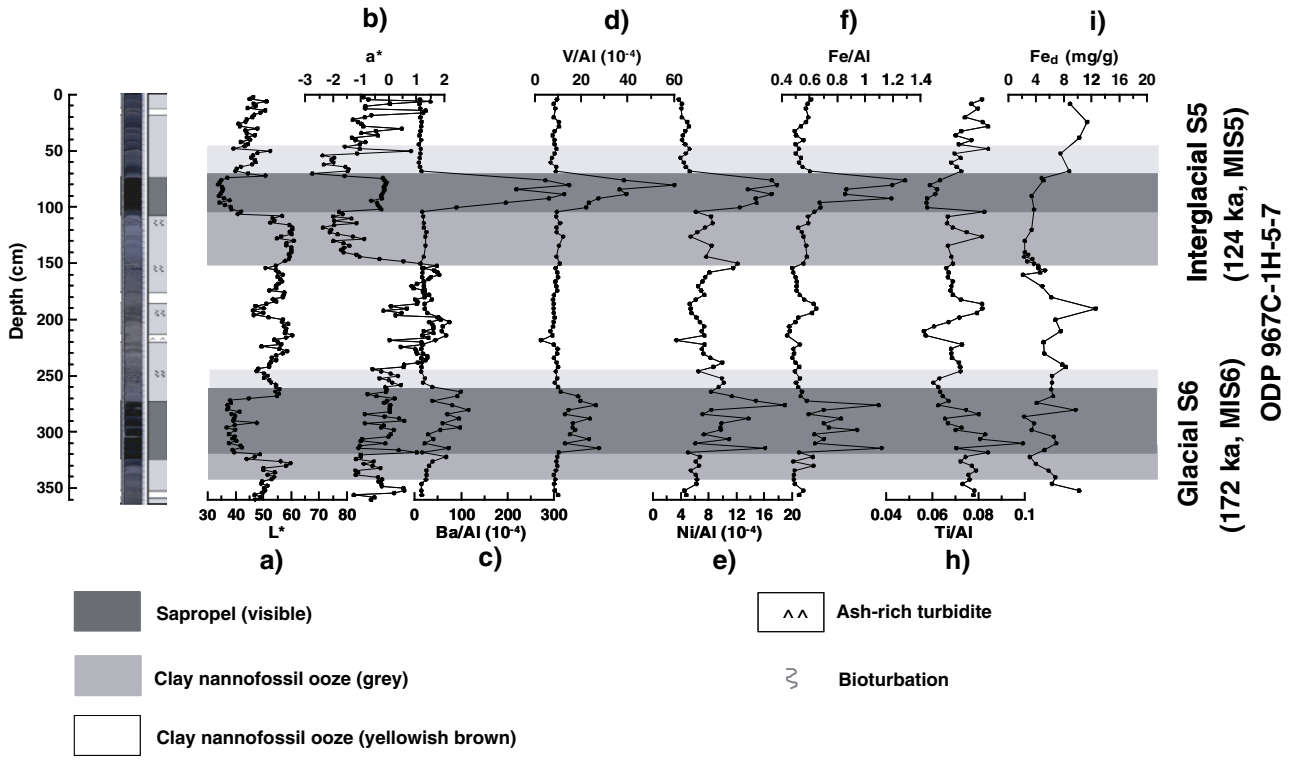

Fig. 3. Stratigraphic log and variations in colour indices (L* and a*) and geochemical parameters for sapropels S5 and S6. The dark grey bars indicate the visible portion of the sapropels. The lighter grey bars above and below the sapropels indicate the positions of oxidation and dissolution intervals, respectively.

field, and has been used as a proxy for the concentration of magnetite, which is the dominant low coercivity ferrimagnetic mineral in eastern Mediterranean sediments (van Santvoort et al., 1997; Roberts et al., 1999; Kruiver and Passier, 2001; Passier et al., 2001; Passier and Dekkers, 2002; Larrasoaña et al., 2003b, 2006). $IRM_{AF@150\ mT}$ was determined by AF demagnetizing at 150 mT an IRM that was imparted in an applied field of 1 T. The coercivity of goethite is typically larger than 1 T, therefore $IRM_{AF@150\ mT}$ is likely to respond only to the concentration of aeolian hematite. The magnetic properties of hematite depend also on the degree of Al-for-Fe isomorphous substitution (Liu et al., 2004). We therefore used the L-ratio, which is defined as $(IRM_{1\ T} + IRM_{-300\ mT})/(IRM_{1\ T} + IRM_{-100\ mT})$ (where $IRM_{-300\ mT}$ and $IRM_{-100\ mT}$ indicate the remanence resulting after applying back-fields of 300 and 100 mT, respectively, to an IRM applied at 1 T), to detect coercivity variations in hematite (Liu et al., 2007). $IRM_{AF@150\ mT}$ is a reliable proxy for hematite content only when the L-ratio is relatively stable.

Room temperature hysteresis loops for all samples were measured using a Princeton Measurements Corporation vibrating sample magnetometer (VSM 3900). The saturation field was 1 T. Saturation magnetization (M_s), saturation remanence (M_{rs}), and coercivity (B_c) were obtained after subtracting the high-field paramagnetic contribution, which was calculated between 0.7 and 1 T. The coercivity of remanence (B_{cr}) was obtained using back-field demagnetization curves. M_{rs}/M_s and B_{cr}/B_c were used to assess the domain state of magnetic minerals (Day et al., 1977; Dunlop, 2002). All rock magnetic properties were measured for all samples at a mean resolution of 2 cm.

Mass concentrations of hematite (Hm) and goethite (Gt) were estimated by DRS on samples that were treated with 1 M HCl to eliminate carbonate and acid-soluble Fe oxide and sulphide phases, and with H_2O_2 to remove organic matter. Spectra were acquired with a Varian Cary 1E spectrophotometer equipped with a $BaSO_4$-coated integrating sphere 73 mm in diameter (Varian Inc., Palo Alto, CA) at a scan rate of 30 nm min^{-1} in 0.5 nm steps. The second derivative of the Kubelka–Munk (K-M) remission function at each wavelength within the 380–660 nm range was calculated using a cubic spline procedure based on segments of 30 data points; this number of points provides good resolution of the characteristic hematite and goethite absorption bands (Torrent et al., 2007). The Hm/(Hm + Gt) ratio was then estimated from the $I_{535}/(I_{535} + I_{425})$ ratio (where I_{535} and I_{425} are the intensities of the hematite and goethite characteristic bands at 535 and 425 nm, respectively, in the second derivative spectrum of the remission function) using the calibration curve of Torrent et al. (2007). Absolute concentrations of hematite and goethite were calculated from the Hm/(Hm + Gt) ratio by assuming that the citrate/bicarbonate/dithionite (CBD)-extractable Fe (Fe_d), which is a quantitative measure of the Fe contained in Fe oxides (Mehra and Jackson, 1960), can be assigned to the Fe contained in stoichiometric hematite and goethite (i.e., $Fe_d = Hm/1.43 + Gt/1.59$). The method of Mehra and Jackson (1960) was used to determine Fe_d except that the extraction temperature was 25 °C and the extraction time was 16 h.

Concentrations of major (wt.%) and minor (ppm) elements were determined using ICP-MS (ELEMENT, Finnigan MAT). Uncertainties in the analysis were $< \pm 5\%$. Elements useful for marking paleoceanographic and diagenetic changes during sedimentation of eastern Mediterranean sediments were normalized by Al to account for changes in clay content (Pruysers et al., 1993; Thomson et al., 1995; Warning and Brumsack, 2000; Wehausen and Brumsack, 2000; Calvert and Fontugne, 2001; Lourens et al., 2001), which results in unit-less ratios. Elemental concentrations and ratios were produced for every second sample, which gives a mean resolution of ca 4 cm.

3. Results

3.1. Geochemical data

Stratigraphic variations of various geochemical parameters for the studied intervals are summarized in Figs. 2 and 3. Ba/Al ratios exhibit peaks within sapropels, with no evidence for Ba enhancement at the

top of the sapropels that might indicate diagenetic remobilization under extremely sulphidic conditions (e.g. Pruysers et al., 1993; Thomson et al., 1995). S1, S6 and S5 are characterized by maximum Ba/Al ratios of 90, 125 and 350×10^{-4}, respectively, which suggest a progressive increase of organic carbon export to the seafloor for these sapropels during their deposition (Pruysers et al., 1993; Thomson et al., 1995; Wehausen and Brumsack, 2000; Calvert and Fontugne, 2001). Higher than background Ba/Al ratios up to 10 cm above visible sapropels mark the original thickness of sapropels prior to their post-depositional oxidation (Pruysers et al., 1993; Thomson et al., 1995; Mercone et al., 2001). Such oxidized parts are evidenced also by distinctively lighter than background colours (higher L* values, where L* indicates lightness, see Sakamoto et al., 1998) coupled with marked changes in the green versus red hue (a*). We hereafter use the term sapropel to indicate the original thickness of sapropels unless otherwise specified. Below sapropels, lighter than background greenish colours (i.e. higher than background L* and low a* values) enable delineation of dissolution intervals whose bases mark the location of downward diffusion fronts of excess sulphide from the sapropels into previously deposited oxic sediments (van Santvoort et al., 1997; Passier et al., 2001; Larrasoaña et al., 2003b).

V/Al ratios are also progressively enhanced for S1, S6 and S5, which suggests progressively greater depletion of bottom water oxygen during their deposition (Figs. 2 and 3) (Warning and Brumsack, 2000). Progressively enhanced sulphidic conditions developed during deposition of S1, S6 and S5, respectively, as demonstrated by Fe and Ni to Al ratios, as a result of the progressively more restricted bottom water ventilation and increased export production (Thomson et al., 1995; van Santvoort et al., 1997; Warning and Brumsack, 2000; Calvert and Fontugne, 2001).

Ti/Al minima, with values as low as 0.06, are found either within visible sapropels (i.e. S1 and S5) and/or within their oxidized parts (i.e. S1 and S6) (Figs. 2 and 3). This indicates minima in aeolian dust inputs during sapropel formation (Wehausen and Brumsack, 2000; Calvert and Fontugne, 2001; Lourens et al., 2001). However, in both the middle of S1 and the lower part of S6, Ti/Al peaks of up to 0.1 are as high as those within non-sapropelic sediments, which are characterized by Ti/Al ratios between 0.07 and 0.09. This indicates that increased aeolian dust inputs prevailed not only between sapropels, but also at certain positions within sapropels. In particular, sapropel S6 has two prominent Ti/Al peaks, between 0.10 and 0.20 m thick, in its middle and lower part. S1 has a peak in its middle part. The relatively low resolution of the geochemical data prevents accurate delineation of the thickness of the Ti/Al peak. Fe_d data oscillate on comparable timescales to Ti/Al ratios. Thus, Fe_d minima of 3–5 mg/g within sapropels broadly coincide with low Ti/Al values, whereas maxima of up to 8–14 mg/g within non-sapropelic sediments coincide with higher Ti/Al values.

3.2. Magnetic and DRS data

ARM and M_s values drop by two orders of magnitude within sapropels and their underlying dissolution intervals, which indicates that virtually all pre-existing magnetite has dissolved under reductive conditions triggered by degradation of organic matter within sapropels and the subsequent downward diffusion of excess sulphide into the underlying sediments (van Santvoort et al., 1997; Roberts et al., 1999; Kruiver and Passier, 2001; Passier et al., 2001; Larrasoaña et al., 2003b, 2006) (Figs. 4 and 5). High B_c and M_{rs}/M_s values within sapropels and dissolution intervals likely result from preferential dissolution of magnetite, which enables relatively higher-coercivity minerals to dominate the hysteresis properties. Down-core ARM and M_s variations indicate that the thickness of dissolution intervals increases progressively between 0.10, 0.20 and 0.45 m for sapropels S1, S6 and S5, respectively.

ARM and M_s values rapidly recover within oxidized sapropels, where they typically reach maximum values (Figs. 4 and 5). M_{rs}/M_s values increase slightly upward within oxidized sapropels. These features point to authigenic formation of magnetite of probable biogenic origin at paleo-oxidation fronts that developed at the top of sapropels when bottom waters reoxygenated after sapropel formation (Kruiver and Passier, 2001; Passier et al., 2001; Larrasoaña et al., 2003b, 2006; Garming et al., 2004). Away from sapropels and associated sediments affected by diagenetic fronts, B_c and M_{rs}/M_s oscillate around 10 mT and 0.2, respectively, which is consistent with the predominance of detrital pseudo-single domain magnetite (Passier and Dekkers, 2002; Garming et al., 2004; Larrasoaña et al., 2008).

κ_{fd}% values indicate high SP contents in S5 and S6 and within their dissolution intervals, and much lower SP contents within S1 (Figs. 4 and 5). Magnetite at these positions has undergone near complete dissolution as indicated by the lowest ARM and M_s values, therefore this SP material is interpreted to consist of fine-grained authigenic greigite. Rowan et al. (2009) demonstrated that greigite growth begins with formation of SP particles. Low ARM and M_s values within sapropels and their dissolution intervals exclude significant growth of stable single domain greigite (Figs. 4 and 5). These data therefore indicate that geochemical conditions, with a large excess of sulphide with respect to available Fe (Kao et al., 2004), favoured formation of SP greigite but not its continued authigenic growth into the stable single domain state.

$IRM_{AF@150\ mT}$ minima within sapropels broadly coincide with Ti/Al and Fe_d minima, which contrast with the higher $IRM_{AF@150\ mT}$, Ti/Al and Fe_d values in non-sapropelic sediments. The overall low $IRM_{AF@150\ mT}$, Ti/Al and Fe_d values within sapropels attest to a reduced aeolian dust supply. In the middle of S1, the base of S5, and the middle and lower part of S6, distinctive $IRM_{AF@150\ mT}$, Ti/Al and Fe_d peaks indicate short periods with enhanced dust contents (Figs. 4 and 5). DRS-determined hematite contents mimic Ti/Al, $IRM_{AF@150\ mT}$ and Fe_d curves, which indicates that sapropels are characterized by low hematite concentrations with the exception of short periods with high dust contents. In contrast, goethite contents are either relatively stable within sapropel S6 or have a slightly increasing trend up-core across sapropels S1 and S5 (Figs. 4 and 5). Our results provide the first evidence for a link between Saharan dust supply and these two antiferromagnetic minerals.

The L-ratio behaves differently for different sapropels (Figs. 4 and 5). For S1 and S6, the L-ratio remains relatively stable, which indicates a consistent source of hematite with minimal post-depositional dissolution. In contrast, the L-ratio oscillates within S5. At the base of the dissolution interval, it increases to a maximum (~0.8) and then gradually decreases to a minimum (~0.5) in the middle of S5. In the oxidized sapropel interval, the L-ratio increases again before rapidly returning to background values (~0.65). Correlation between the L-ratio and $IRM_{AF@150\ mT}$ is illustrated in Fig. 6. When $IRM_{AF@150\ mT}<0.1$ A/m (as for S5), the L-ratio is positively correlated with $IRM_{AF@150\ mT}$. When $IRM_{AF@150\ mT}>\sim0.1$ A/m, the L-ratio slightly decreases with increasing $IRM_{AF@150\ mT}$ for the interglacial sapropels S1 + S5, but remains relatively constant for the glacial sapropel S6. Overall, L-ratios oscillate around 0.7 for the whole range of $IRM_{AF@150\ mT}$ variations. This indicates that $IRM_{AF@150\ mT}$ can be used as a proxy for hematite contents throughout most of the studied sapropels but the exception of the lower part of S5, where $IRM_{AF@150\ mT}<0.1$ A/m and L-ratio < 0.65 are simultaneously found.

The ash-rich turbidite located just above S6 has a geochemical and magnetic signature similar to that of sapropels (i.e. high κ_{fd}% and low ARM, M_s, Ti/Al, and $IRM_{AF@150\ mT}$; Figs. 2–5). We infer that this turbidite layer triggered diagenetic reactions similar to those associated with sapropels during degradation of organic matter within the turbidite (see Robinson et al., 2000).

4. Discussion

Down-core variations of the most relevant parameters studied are summarized in Figs. 7 and 8, and provide a basis for discussing the

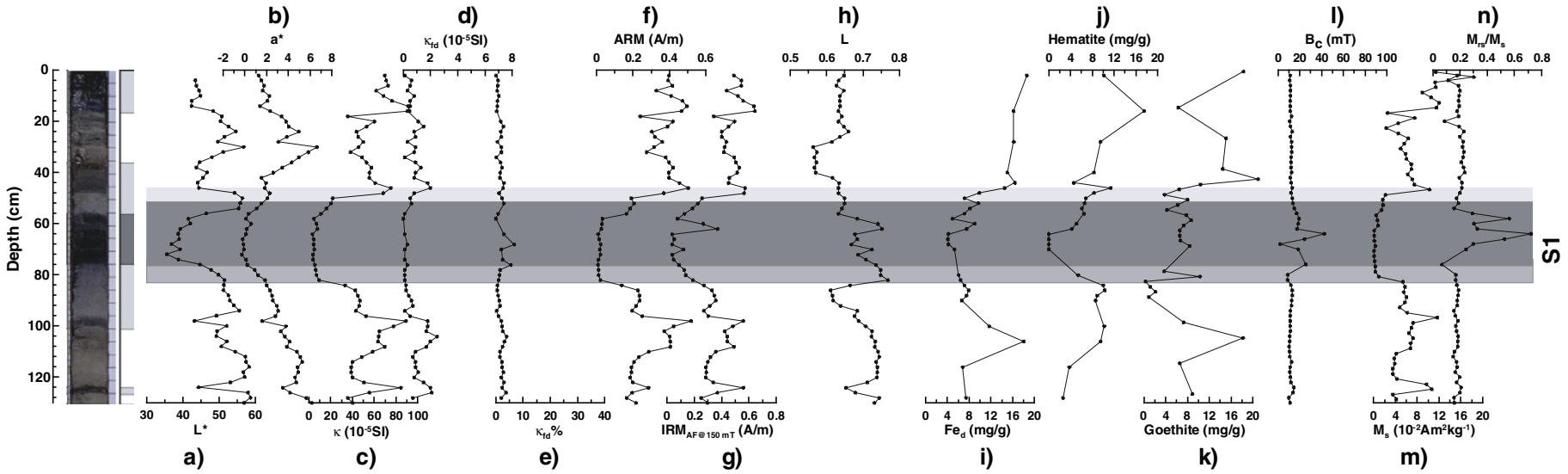

Fig. 4. Stratigraphic log and variations in colour indices (L* and a*) and magnetic parameters for sapropel S1. The dark grey bar indicates the visible portion of the sapropel. The lighter grey bars above and below the sapropel indicate the positions of oxidation and dissolution intervals, respectively. The shading is as in Fig. 2.

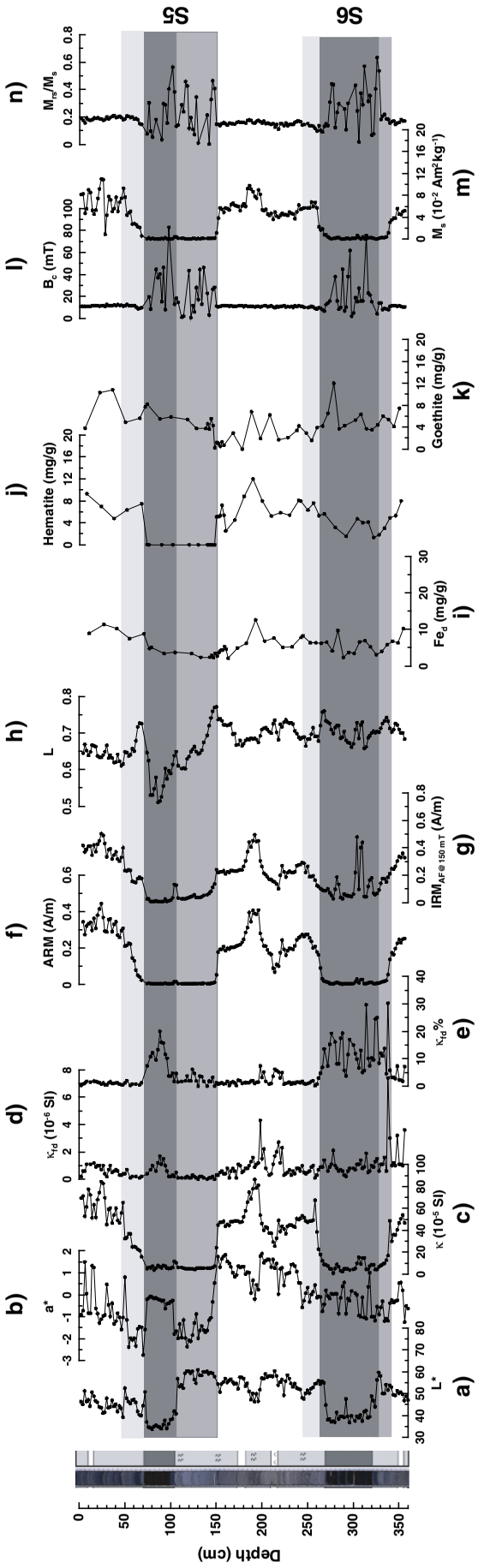

Fig. 5. Stratigraphic log and variations in colour indices (L^* and a^*) and magnetic parameters for sapropels S5 and S6. The shading is as in Fig. 3.

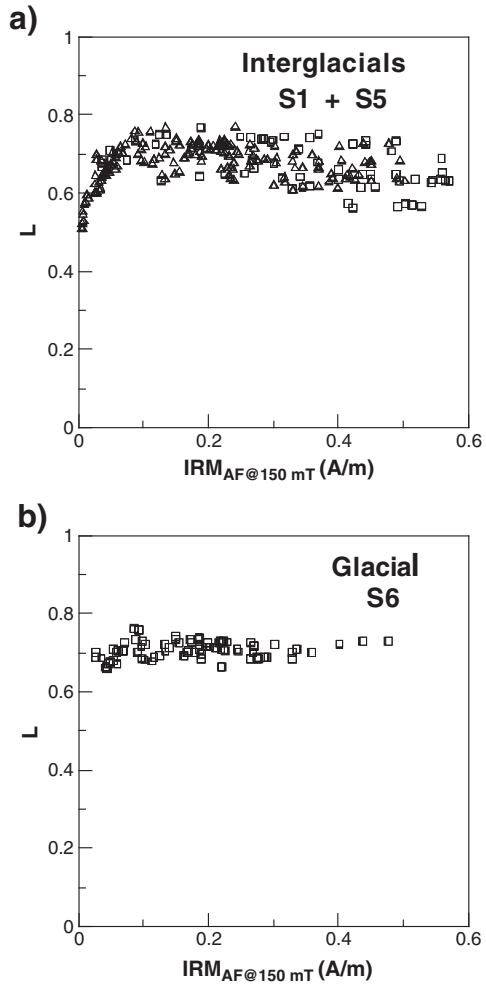

Fig. 6. Correlation between the L-ratio (Liu et al., 2007) and $IRM_{AF@150\ mT}$ for (a) interglacial sapropels S1 and S5, and (b) glacial sapropel S6. In a, rectangles and triangles indicate samples from S1 and S5, respectively.

paleoclimatic implications of depositional and diagenetic signals associated with the studied sapropels.

4.1. Diagenetic signals and their paleoclimatic implications

For sapropels that accumulated at a given setting with similar sedimentation rates, which is the case for sapropels S1, S5 and S6 at Site 967 (Emeis et al., 2000), geochemical and magnetic parameters are likely to provide a reliable relative view of paleoclimatic and paleoceanographic conditions that govern sapropel deposition. Magnetic parameters indicate that the thickness of dissolution intervals increase progressively between 0.10, 0.20 and 0.45 m for sapropels S1, S6 and S5, respectively (Figs. 7 and 8), and also that S1 has a much lower SP content than S5 and S6. These results indicate that progressively enhanced sulphidic conditions developed during formation of S1, S6 and S5, respectively, which is confirmed by their progressive enhancement in Ni to Al ratios. Such enhanced sulphidic conditions developed under periods of progressively increased export productivities and enhanced stagnation of bottom waters for S1, S6 and S5, as indicated by Ba and V to Al ratios, and appear to be linked to enhanced TOC values.

Oxygen and Nd isotopic data from eastern Mediterranean planktic foraminifera indicate that deposition of interglacial S5 was predominantly linked to reactivation of northern Sahara drainages rather than to increased riverine fluxes from the northern borderlands of the eastern Mediterranean, thereby supporting a dominant remote effect of an intensified African monsoon on sapropel formation (Rohling et al., 2002a, 2004; Scrivner et al., 2004; Osborne et al., 2010). Astronomical solutions give maximum summer insolation values at 30°N of about 392, 401 and 405 Wm^{-2} for the time intervals represented by sapropels S1, S6 and S5, respectively (Laskar et al., 2004). This sequence of increased low-latitude insolation values matches the sequence of increased productivities and decreased bottom water ventilations, as well as the concomitant strengthening of sulphate-reducing conditions, inferred for S1, S5 and S6 from our geochemical and magnetic datasets. No link is found, however, with the prevailing glacial (S6) or interglacial (S1, S5) background conditions at the time of sapropel formation. Studies of eastern Mediterranean sediments deposited at accumulation rates comparable to those of Site 967 have shown that previous glacial stages contain intervals with geochemical and/or magnetic signatures identical

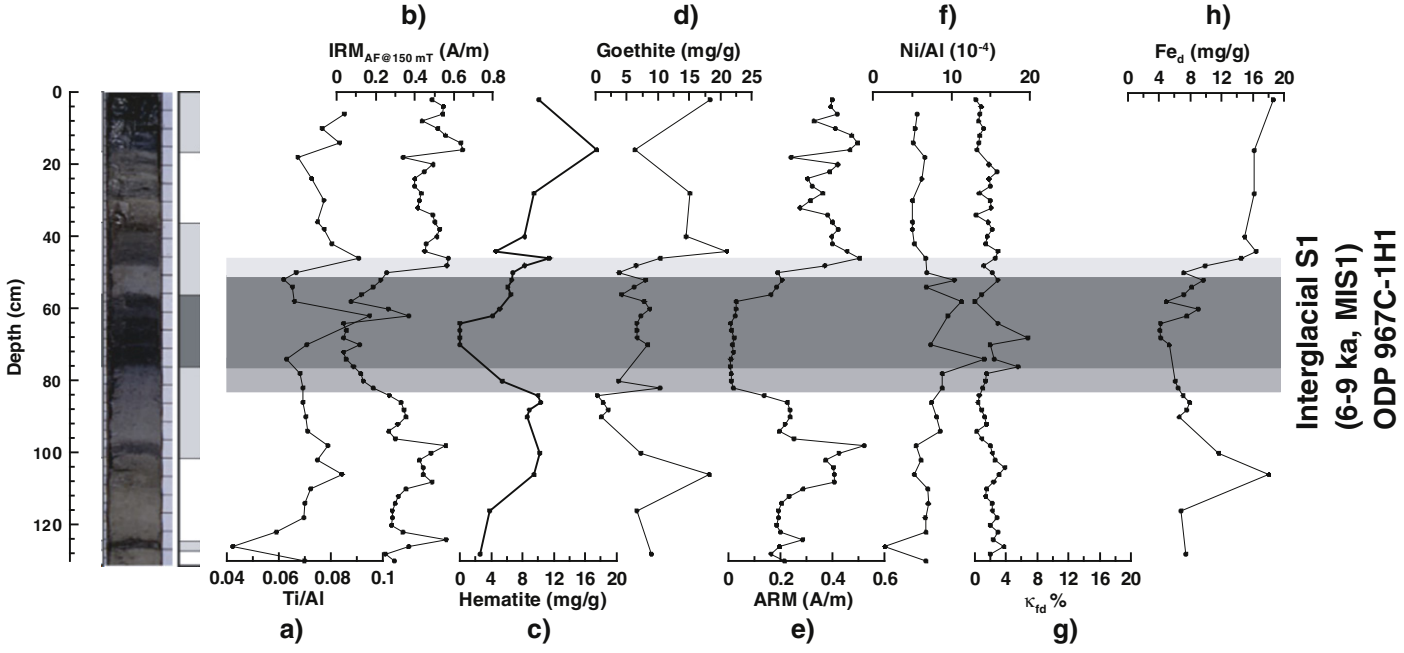

Fig. 7. Stratigraphic variations of the most relevant parameters for sapropel S1. The shading is as in Fig. 2.

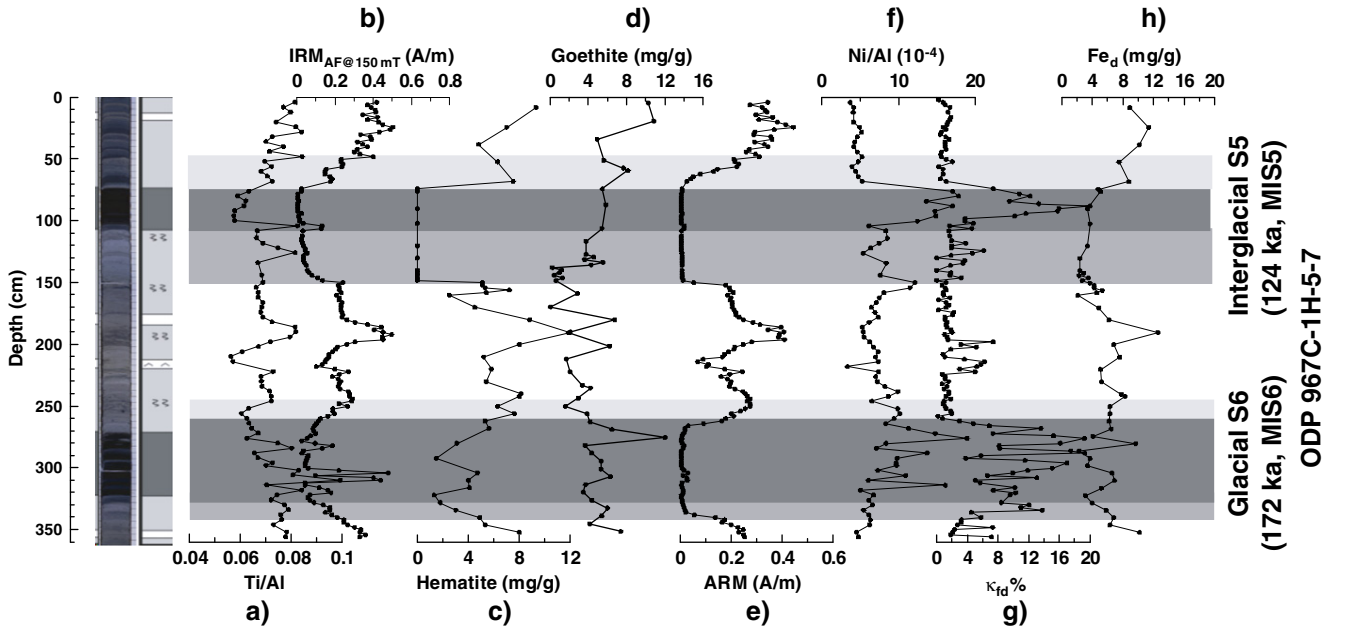

Fig. 8. Stratigraphic variations of the most relevant parameters for sapropels S5 and S6. The shading is as in Fig. 3.

to those of sapropels. This is the case for an oxidized sapropel that formed during Si26, which has been identified within MIS 8 in cores KC01B (van Santvoort et al., 1997) and MD 84641 (Calvert and Fontugne, 2001) on the basis of its high Ba and V contents as well as its low ARM values. A similar situation was found for another oxidized sapropel identified in core KC01B within MIS 16 (Si60) (van Santvoort et al., 1997), which also has high Ba and V contents and low ARM intensities. Our results and those presented in the above-cited studies indicate that sapropels formed regardless of glacial or interglacial background conditions. These results therefore reinforce the idea of a dominant low-latitude forcing mechanism that controlled sapropel formation, not only during interglacial periods typified by S5 (Scrivner et al., 2004; Osborne et al., 2008, 2010) but also during glacial periods, provided that insolation reached values high enough to promote strengthening of the African monsoon and reactivation of northern Sahara drainages.

4.2. Depositional signals and their paleoclimatic implications

A combination of magnetic, geochemical and DRS data enables detailed assessment of the effects of diagenesis on hematite and goethite contents, which is a prerequisite for validating their reliability as recorders of paleoclimatic signals. Parallel variations in IRM$_{AF@150\ mT}$, Fe$_d$, Ti/Al and hematite data throughout most of the studied intervals demonstrate that IRM$_{AF@150\ mT}$ is largely unaffected by hematite dissolution in this non-steady state diagenetic environment so that it represents a reliable proxy for aeolian contents in this setting. The only exception is in the lower part of S5 and its underlying dissolution interval, where hematite dissolution is indicated by a parallel decrease in IRM$_{AF@150\ mT}$ and L-ratios and by striking coincidence of near-zero IRM$_{AF@150\ mT}$ values within the whole dissolution interval (Figs. 7 and 8). Even in this case, the relative minimum in IRM$_{AF@150\ mT}$ is only shifted a few tens of centimetres (i.e. millennia) from its original position, which will not affect substantially paleoclimatic interpretations of long sedimentary sequences that require resolutions at precessional timescales.

A combination of IRM$_{AF@150\ mT}$, Ti/Al, Fe$_d$, hematite and goethite curves enables detection of down-core variations in the amount of aeolian dust and discrimination of whether hematite or goethite dominates the magnetic mineralogy of the dust fraction. It should be noted that the following discussion is only valid in the absence of significant hematite dissolution, which seems to be the case throughout most of the studied sapropels and their underlying dissolution intervals as inferred from IRM$_{AF@150\ mT}$ and L-ratios. Lack of diagenetic remobilization of Ba around S1, S5 and S6 indicates that these sapropels never underwent extremely sulphidic conditions at the studied site in response to moderate TOC contents. For S5, this is somewhat surprising, given that organic geochemical evidence of truly euxinic (free H_2S) conditions in the upper water column has been reported for that sapropel in western Levantine ODP Site 971A (Rohling et al., 2006) and SE Aegean core LC21 (Marino et al., 2007). Other sapropels recovered at Site 967 and in other cores (e.g. ODP Site 964, 966 and 969; KC01B), which formed under similarly low accumulation rates of <~5 cm/kyr, have either much higher (10–30 wt.%) TOC contents and/or contain evidence of diagenetic Ba remobilization, which point to extremely sulphidic conditions during deposition (van Santvoort et al., 1997; Roberts et al., 1999; Nijenhuis and de Lange, 2000; Nijenhuis et al., 2001). Reductive dissolution of hematite is likely to be pervasive within at least parts of those strongly anoxic sapropels and their associated dissolution intervals. Concerning goethite, its concentrations do not change through the studied sapropels and underlying dissolution intervals in a way that can be attributed to reductive dissolution, even in sapropel S5. This can be explained by substitution of Fe by Al in goethite, which can reach up to ~30 mol% (Cornell and Schwertmann, 2003). Similar to the case for titanomagnetite (Garming et al., 2005), Al-for-Fe substitution decreases the number of Fe^{3+} ions (the electron acceptor under anaerobic conditions, Dillon and Bleil (2006)). High Al-for-Fe substitution therefore means that aluminous goethite can survive in the relatively enhanced sulphidic environments such as those of sapropel S5, and probably also of other sapropels that underwent stronger sulphidic conditions.

A common feature within all three studied sapropels, especially for S1 and S5, is a broad minimum in IRM$_{AF@150\ mT}$, Ti/Al and Fe$_d$ values (Figs. 7 and 8). This indicates low overall dust contents regardless of underlying glacial (S6) or interglacial (S1, S5) conditions. Similarly low Ti/Al ratios, which are indicative of decreased dust inputs, are found in glacial S6 in core MD 84641 (Calvert and Fontugne, 2001). Based on similar observations, previous studies have suggested that dust production in the Sahara is largely independent of high-latitude climate conditions, so that it responds mainly to African monsoon dynamics, which are driven by the amount of solar energy received at low latitudes (Larrasoaña et al., 2003a; Trauth et al., 2009). Another common feature in the three studied sapropels is that the hematite content mimics IRM$_{AF@150\ mT}$ and Fe$_d$ values, so that it has overall minima of

<2 mg/g within sapropels. In contrast, goethite undergoes no systematic variations across the studied intervals. Hematite formation in soils and surface continental sediments is favoured by hot and dry conditions such as those in the Sahara, whereas goethite formation is favoured by the relatively wetter conditions of subtropical savannahs within and south of the Sahel (Maher, 1986; Balsam et al., 1995). We therefore interpret the overall high hematite content of sediments between sapropels as indicative of present-day-like desert conditions in the NE Sahara, which is the main dust source for the eastern Mediterranean (e.g. Prospero et al., 2002). Decreased hematite contents within sapropels attest to northward expansion of savannah landscapes into the NE Sahara during boreal summer insolation maxima, which dampened dust production (Larrasoaña et al., 2003a). The occurrence of goethite within sapropels and surrounding sediments reflects additional aeolian entrainment from goethite-rich iron crusts that formed in the NE Sahara during previous wetter phases (Nahon, 1980) or from savannahs south of the Sahara. Northward expansion of savannahs during "green Sahara" periods and associated formation of goethite-rich crusts might explain the slight increasing shift to higher goethite contents observed for interglacial sapropels S1 and S5, when wettest regional conditions would have favoured goethite formation.

Combined magnetic, geochemical and DRS data enable resolution of short-lived fluctuations in aeolian dust input within sapropels S1 and S6. The most conspicuous pattern within S1 is the presence of $IRM_{AF@150\ mT}$, Ti/Al and Fe_d peaks at a depth of ~60 cm (Fig. 7), which, considering the thickness of its oxidized part, corresponds to the middle of S1. Deposition of S1 was interrupted for a few centuries due to abrupt and transient intensification of bottom water ventilation at about 8.5–8.0 kyr BP (Rohling et al., 1997, 2002b; Mercone et al., 2001; Casford et al., 2003; Marino et al., 2009), which was, in turn, driven by increased intensity and frequency of cold spells over the northern sectors of the eastern Mediterranean (Rohling et al., 2002b; Casford et al., 2003). In high sedimentation settings, this interruption is evident as a less organic-rich layer with contrasting geochemical and paleontological signatures compared to the sapropel (Mercone et al., 2000, 2001; Casford et al., 2003). In low sedimentation settings (<~5 cm/kyr) such as at ODP Site 967, the short interruption is blurred and does not leave visual evidence of its presence (Mercone et al., 2000). We interpret $IRM_{AF@150\ mT}$, Ti/Al and Fe_d peaks in the middle of S1 as evidence for a shift in paleoclimatic conditions associated with the interruption of S1. Increased production of dust at that time attests to a transient return to arid conditions in the northern Sahara at 8.5–8.0 kyr BP, as has also been shown by Early–Middle Holocene lake level data (Gasse, 2000). Noticeably, such a shift would not have been identified in Site 967 if rock magnetic and geochemical analyses had not been carried out on discrete samples, given that it was hardly recorded in u-channel-based (i.e. smoothed) rock magnetic studies (see Larrasoaña et al., 2003a).

The most conspicuous features within S6 are two $IRM_{AF@150\ mT}$, Fe_d, and Ti/Al peaks (Fig. 8), which, considering the thickness of its oxidized part, correspond to the lower and middle sapropel. Based on visual inspection of the sediment cores, only one sapropel interruption has been reported within S6 (Calvert and Fontugne, 2001). However, up to three centennial-scale intervals characterized by bottom-water ventilation events have been identified in the middle of S6 in ODP Site 971 on the basis of detailed benthic foraminiferal abundance distributions, which are not accompanied by visual evidence for an interruption (Casford et al., 2003). We interpret the two short periods of enhanced dust supply revealed by $IRM_{AF@150\ mT}$ and Fe_d data as correlative to the two most intense periods of bottom-water ventilation reported by Casford et al. (2003). DRS data enable identification of hematite and goethite contents. It appears that the lowermost dust peak in S6 is dominated by hematite, whereas the second is dominated by goethite (Fig. 8). The hematite-dominated peak likely indicates a return to desert climate conditions in the NE Sahara after a short shift to wetter conditions during the onset of S6 accumulation, when goethite formation was not yet promoted. In contrast, goethite dominance in the second dust peak likely reflects stabilization of NE Saharan savannah landscapes, and hence *in situ* goethite production.

Previous studies have linked sapropel interruptions to an increased intensity and frequency of cold spells over the eastern Mediterranean and its northern borderlands (Rohling et al., 2002b; Casford et al., 2003). Our data from S1 and S6 provide a link between short-lived periods of sapropel interruption and increased dust contents that are indicative of a transient return to arid conditions in the northern Sahara. These results therefore suggest that periods of sapropel interruption involved reorganization of atmospheric circulation not only over the eastern Mediterranean basin and its northern borderlands, but also over the subtropical regions of North Africa. In addition to S6, short-lived periods of higher dust inputs and decreased TOC and Ba contents have been identified also within S8, which accumulated during Si20 within interglacial MIS 7 (Calvert and Fontugne, 2001), and within some Pliocene sapropels such as the Si156 sapropel (Nijenhuis and de Lange, 2000). This reinforces the notion, typified by the interruption of interglacial S1, that short-lived events involving the reorganization of atmospheric circulation over the whole circum-Mediterranean region were not restricted to periods of large polar ice volume.

5. Conclusions

Our results demonstrate that different magnetic minerals within sapropels reveal contrasting responses to different depositional and diagenetic processes. Reductive dissolution of detrital (likely aeolian) magnetite and authigenic formation of superparamagnetic greigite within sapropels and dissolution intervals are linked to the strength of sulphidic conditions during sapropel formation. These conditions, in turn, appear to be driven by maximum boreal summer insolation regardless of glacial (S6) or interglacial (S1, S5) climates. In contrast, goethite and, to a lesser extent hematite, appear to be largely unaffected by reductive dissolution. These minerals can therefore be used to trace Saharan dust inputs into the Mediterranean Sea.

Regardless of the prevailing paleoclimatic background conditions (glacial or interglacial), all three studied sapropels have low overall dust contents. However, we have observed one and two short periods of high dust contents in the middle of S1 and in lower S6, respectively, that may have formed concurrently with centennial-scale high latitude cooling events identified within these sapropels. The fact that such short-lived large-scale atmospheric reorganizations affected not only glacial sapropels, but also interglacial and Pliocene sapropels, reinforces the idea that they were not restricted to periods of large polar ice volume. Our results indicate that such cooling events resulted in a reorganization of the atmospheric circulation not only over the eastern Mediterranean Sea and its northern borderlands as shown by previous studies, but also over the subtropical regions of North Africa.

Acknowledgements

This study was supported by the National Natural Science Foundation of China (grants 41025013, 40974036 and 40821091) and the CAS/SAFEA International Partnership Program for Creative Research Teams. Q.S. Liu was supported by a Marie-Curie Fellowship (IIF) funded by the European Commission, proposal number 7555, when this work was started and he acknowledges further support from the 100-talent Program of the Chinese Academy of Sciences. J. Torrent was partly supported by Spain's Ministerio de Educación y Ciencia, projects AGL2006-10927 and CGL2010-15067, and the European Regional Development Fund. This study also contributes to the Natural Environment Research Council project NE/E01531X/1. We are grateful to two anonymous reviewers, whose criticisms helped to significantly improve the manuscript.

References

Balsam, W.L., Otto-Bliesner, B.L., Deaton, B.C., 1995. Modern and last glacial maximum eolian sedimentation patterns in the Atlantic ocean interpreted from sediment iron oxide content. Paleoceanography 10, 493–507.

Calvert, S.E., Fontugne, M.R., 2001. On the late Pleistocene–Holocene sapropel record of climatic and oceanographic variability in the eastern Mediterranean. Paleoceanography 16, 78–94.

Casford, J.S.L., Rohling, E.J., Abu-Zied, R.H., Fontanier, C., Jorissen, F.J., Leng, M.J., Schmiedl, G., Thomson, J., 2003. A dynamic concept for eastern Mediterranean circulation and oxygenation during sapropel formation. Palaeogeography, Palaeoclimatology, Palaeoecology 190, 103–119.

Cornell, R.M., Schwertmann, U., 2003. The Iron Oxides, 2nd Ed. John Wiley & Sons, Weinheim, Germany. 664 pp.

Day, R., Fuller, M., Schmidt, V.A., 1977. Magnetic hysteresis properties of synthetic titanomagnetites. Physics of the Earth and Planetary Interiors 13, 260–266.

Dearing, J.A., Hay, K.L., Baban, S.M.J., Huddleston, A.S., Wellington, E.M.H., Loveland, P.J., 1996. Magnetic susceptibility of soil: an evaluation of conflicting theories using a national data set. Geophysical Journal International 127, 728–734.

Dillon, M., Bleil, U., 2006. Rock magnetic signatures in diagenetically altered sediments from the Niger deep-sea fan. Journal of Geophysical Research 111, B03105. doi:10.1029/2004JB003540.

Dunlop, D.J., 2002. Theory and application of the Day plot (M_{rs}/M_s vs. H_{cr}/H_c). 1. Theoretical curves and tests using titanomagnetite data. Journal of Geophysical Research 107, 2056. doi:10.1029/2001JB000486.

Emeis, K.C., Schulz, H.M., Struck, U., Sakamoto, T., Doose, H., Erlenkeuser, H., Howell, M., Kroon, D., Paterne, M., 1998. Stable isotope and alkenone temperature records of sapropels from sites 964 and 967: constraining the physical environment of sapropel formation in the eastern Mediterranean Sea. In: Robertson, A.H.F., Emeis, K.-C., Richter, C., Camerlenghi, A. (Eds.), Proceedings of the Ocean Drilling Program: Scientific Results, 160, pp. 309–331.

Emeis, K.C., Sakamoto, T., Wehausen, R., Brumsack, H.J., 2000. The sapropel record of the eastern Mediterranean Sea—results of Ocean Drilling Program Leg 160. Palaeogeography, Palaeoclimatology, Palaeoecology 158, 371–395.

Garming, J.F.L., de Lange, G.J., Dekkers, M.J., Passier, H.F., 2004. Changes in magnetic parameters after sequential iron phase extraction of eastern Mediterranean sapropel S1 sediments. Studia Geophysica et Geodaetica 48, 345–362.

Garming, J.F.L., Bleil, U., Riedinger, N., 2005. Alteration of magnetic mineralogy at the sulphate–methane transition: analysis of sediments from the Argentine continental slope. Physics of the Earth and Planetary Interiors 151, 290–308.

Gasse, F., 2000. Hydrological changes in the African tropics since the Last Glacial Maximum. Quaternary Science Reviews 19, 189–211.

Heslop, D., von Dobeneck, T., Höcker, M., 2007. Using non-negative matrix factorization in the 'unmixing' of diffuse reflectance spectra. Marine Geology 241, 63–78.

Hilgen, F.J., 1991. Astronomical calibration of Gauss to Matuyama sapropels in the Mediterranean and implication for the Geomagnetic Polarity Time Scale. Earth and Planetary Science Letters 104, 226–244.

Kao, S.J., Horng, C.S., Roberts, A.P., Liu, K.K., 2004. Carbon–sulfur–iron relationships in sedimentary rocks from southwestern Taiwan: influence of geochemical environment on greigite and pyrrhotite formation. Chemical Geology 203, 153–168.

Köhler, C.M., Heslop, D., Dekkers, M.J., Krijgsman, W., van Hinsbergen, D.J.J., von Dobeneck, T., 2008. Tracking provenance change during the late Miocene in the eastern Mediterranean using geochemical and environmental magnetic parameters. Geochemistry, Geophysics, Geosystems 9, Q12018. doi:10.1029/2008GC002127.

Kotthoff, U., Pross, J., Müller, U.C., Peyron, O., Schmiedl, G., Schulz, H., Bordon, A., 2008. Climate dynamics in the borderlands of the Aegean Sea during formation of sapropel S1 deduced from a marine pollen record. Quaternary Science Reviews 27, 832–845.

Krom, M.D., Cliff, R.A., Eijsink, L.M., Herut, B., Chester, R., 1999. The characterization of Saharan dust and Nile particulate matter in surface sediments from the Levantine basin using Sr isotopes. Marine Geology 155, 319–330.

Kruiver, P.P., Passier, H.F., 2001. Coercivity analysis of magnetic phases in sapropel S1 related to variations in redox conditions, including an investigation of the *S* ratio. Geochemistry, Geophysics, Geosystems 2, 1063. doi:10.1029/2001GC000181.

Langereis, C.G., Dekkers, M.J., de Lange, G.J., Paterne, M., van Santvoort, P.J.M., 1997. Magnetostratigraphy and astronomical calibration of the last 1.1 Myr from an eastern Mediterranean piston core and dating of short events in the Brunhes. Geophysical Journal International 129, 75–94.

Larrasoaña, J.C., Roberts, A.P., Rohling, E.J., Winklhofer, M., Wehausen, R., 2003a. Three million years of monsoon variability over the northern Sahara. Climate Dynamics 21, 689–698.

Larrasoaña, J.C., Roberts, A.P., Stoner, J.S., Richter, C., Wehausen, R., 2003b. A new proxy for bottom-water ventilation in the eastern Mediterranean based on diagenetically controlled magnetic properties of sapropel-bearing sediments. Palaeogeography, Palaeoclimatology, Palaeoecology 190, 221–242.

Larrasoaña, J.C., Roberts, A.P., Hayes, A., Wehausen, R., Rohling, E.J., 2006. Detecting missing beats in the Mediterranean climate rhythm from magnetic identification of oxidized sapropels (Ocean Drilling Program Leg 160). Physics of the Earth and Planetary Interiors 156, 283–293.

Larrasoaña, J.C., Roberts, A.P., Rohling, E.J., 2008. Magnetic susceptibility of eastern Mediterranean marine sediments as a proxy for Saharan dust supply? Marine Geology 254, 224–229.

Laskar, J., Robutel, P., Joutel, F., Gastineau, M., Correia, A.C.M., Levrard, B., 2004. A long term numerical solution for the insolation quantities of the Earth. Astronomy and Astrophysics 428, 261–285.

Liu, Q.S., Torrent, J., Yu, Y.J., Deng, C.L., 2004. Mechanism of the parasitic remanence of aluminous goethite [alpha-(Fe, Al)OOH]. Journal of Geophysical Research 109, B12106. doi:10.1029/2004JB003352.

Liu, Q.S., Roberts, A.P., Torrent, J., Horng, C.-S., Larrasoaña, J.C., 2007. What do the HIRM and S-ratio really measure in environmental magnetism? Geochemistry, Geophysics, Geosystems 8, Q09011. doi:10.1029/2007GC001717.

Lourens, L.J.A., Antonarakou, F.J., Hilgen, F.J., Van Hoof, A.A.M., Vergnaud-Grazzini, C., Zachariasse, W.J., 1996. Evaluation of the Plio-Pleistocene astronomical timescale. Palaeoceanography 11, 391–431.

Lourens, L.J., Wehausen, R., Brumsack, H.J., 2001. Geological constraints on tidal dissipation and dynamical ellipticity of the Earth over the past three million years. Nature 409, 1029–1033.

Maher, B.A., 1986. Characterisation of soils by mineral magnetic measurements. Physics of the Earth and Planetary Interiors 42, 76–92.

Marino, G., Rohling, E.J., Rijpstra, W.I., Sangiorgi, F., Schouten, S., Sinninghe Damsté, J.S., 2007. Aegean Sea as driver for hydrological and ecological changes in the eastern Mediterranean. Geology 35, 675–678.

Marino, G., Rohling, E.J., Sangiorgi, F., Hayes, A., Casford, J.S.L., Lotter, A.F., Kucera, M., Brinkhuis, H., 2009. Early and middle Holocene in the Aegean Sea: interplay between high and low latitude climate variability. Quaternary Science Reviews 28, 3246–3262.

Mehra, O.P., Jackson, M.L., 1960. Iron oxide removal from soils and clays by a dithionite–citrate system buffered with sodium bicarbonate. Clays and Clay Minerals 7, 317–327.

Mercone, D., Thomson, J., Croudace, I.W., Siani, G., Paterne, M., Troelstra, S., 2000. Duration of S1, the most recent sapropel in the eastern Mediterranean Sea, as indicated by accelerator mass spectrometry radiocarbon and geochemical evidence. Paleoceanography 15, 336–347.

Mercone, D., Thomson, J., Abu-Zied, R.H., Croudace, I.W., Rohling, E.J., 2001. High-resolution geochemical and micropalaeontological profiling of the most recent eastern Mediterranean sapropel. Marine Geology 177, 25–44.

Nahon, D., 1980. Soil accumulations and climatic variations in western Sahara. Palaeoecology of Africa and of the Surrounding Islands and Antarctica (Balkema, Cape Town, South Africa) 12, 63–68.

Nijenhuis, I.A., de Lange, G.J., 2000. Geochemical constraints on Pliocene sapropel formation in the eastern Mediterranean. Marine Geology 163, 41–63.

Nijenhuis, I.A., Becker, J., de Lange, G.J., 2001. Geochemistry of coeval marine sediments in Mediterranean ODP cores and a land section: implications for sapropel formation models. Palaeogeography, Palaeoclimatology, Palaeoecology 165, 97–112.

Oldfield, F., Maher, B.A., Donoghue, J., Pierce, J., 1985. Particle-size related, mineral magnetic source-sediment linkages in the Rhode River catchment, Maryland, USA. Journal of the Geological Society of London 142, 1035–1046.

Osborne, A.H., Vance, D., Rohling, E.J., Barton, N., Rogerson, M., Fello, N., 2008. A humid corridor across the Sahara for the migration "Out of Africa" of early modern humans 120,000 years ago. Proceedings of the National Academy of Sciences 105, 16,444–16,447.

Osborne, A.H., Marino, G., Vance, D., Rohling, E.J., 2010. Eastern Mediterranean surface water Nd during Eemian sapropel S5: monitoring northerly (mid-latitude) versus southerly (sub-tropical) fresh water conditions. Quaternary Science Reviews 29, 2473–2483.

Passier, H.F., Dekkers, M.J., 2002. Iron oxide formation in the active oxidation front above sapropel S1 in the eastern Mediterranean Sea as derived from low-temperature magnetism. Geophysical Journal International 150, 230–240.

Passier, H.F., de Lange, G.J., Dekkers, M.J., 2001. Magnetic properties and geochemistry of the active oxidation front and the youngest sapropel in the eastern Mediterranean Sea. Geophysical Journal International 145, 604–614.

Prospero, J.M., Ginoux, P., Torres, O., Nicholson, S.E., Gill, T.E., 2002. Environmental characterization of global sources of atmospheric soil dust identified with the Nimbus 7 Total Ozone Mapping Spectrometer (TOMS) absorbing aerosol product. Reviews of Geophysics 40, 1002. doi:10.1029/2000RG000095.

Pruysers, P.A., de Lange, G.J., Middelburg, J.J., Hydes, D.J., 1993. The diagenetic formation of metal-rich layers in sapropel-containing sediments in the eastern Mediterranean. Geochimica et Cosmochimica Acta 57, 527–536.

Roberts, A.P., 2006. High-resolution magnetic analysis of sediment cores: strengths, limitations and strategies for maximizing the value of long-core magnetic data. Physics of the Earth and Planetary Interiors 156, 162–178.

Roberts, A.P., Stoner, J.S., Richter, C., 1999. Diagenetic magnetic enhancement of sapropels from the eastern Mediterranean Sea. Marine Geology 153, 103–116.

Roberts, A.P., Florindo, F., Larrasoaña, J.C., O'Regan, M.A., Zhao, X., 2010. Complex polarity pattern at the former Plio-Pleistocene global stratotype section at Vrica (Italy): remagnetization by magnetic iron sulphides. Earth and Planetary Science Letters 292, 98–111.

Robinson, S.G., Sahota, J.T.S., Oldfield, F., 2000. Early diagenesis in North Atlantic abyssal plain sediments characterised by rock-magnetic and geochemical indices. Marine Geology 163, 77–107.

Rohling, E.J., 1994. Review and new aspects concerning the formation of eastern Mediterranean sapropels. Marine Geology 122, 1–28.

Rohling, E.J., Gieskes, W.W.C., 1989. Late Quaternary changes in Mediterranean intermediate water density and formation rate. Paleoceanography 4, 531–545.

Rohling, E.J., Hilgen, F.J., 1991. The eastern Mediterranean climate at times of sapropel formation: a review. Geologie en Mijnbouw 70, 253–264.

Rohling, E.J., Jorissen, F.J., de Stigter, H.C., 1997. 200 year interruption of Holocene sapropel formation in the Adriatic Sea. Journal of Micropalaeontology 16, 97–108.

Rohling, E.J., Cane, T.R., Cooke, S., Sprovieri, M., Bouloubassi, I., Emeis, K.C., Schiebel, R., Kroon, D., Jorissen, F.J., Lorre, A., Kemp, A.E.S., 2002a. African monsoon variability during the previous interglacial maximum. Earth and Planetary Science Letters 202, 61–75.

Rohling, E.J., Mayewski, P.A., Abu-Zied, R.H., Casford, J.S.L., Hayes, A., 2002b. Holocene atmosphere–ocean interactions: records from Greenland and the Aegean Sea. Climate Dynamics 18, 587–593.

Rohling, E.J., Sprovieri, M., Cane, T., Casford, J.S.L., Cooke, S., Emeis, K.C., Schiebel, R., Rogerson, M., Hayes, A., Jorissen, F.J., Kroon, D., 2004. Reconstructing past planktic foraminiferal habitats using stable isotope data: a case history for the Mediterranean sapropel S5. Marine Micropaleontology 50, 89–123.

Rohling, E.J., Hopmans, E.C., Damste, J.S.S., 2006. Water column dynamics during the last interglacial anoxic event in the Mediterranean (sapropel S5). Paleoceanography 21, PA4101. doi:10.1029/2005PA001237.

Rossignol-Strick, M., 1983. African monsoons, an immediate climate response to orbital insolation. Nature 304, 46–49.

Rowan, C.J., Roberts, A.P., Broadbent, T., 2009. Paleomagnetic smoothing and magnetic enhancement in marine sediments due to prolonged early diagenetic growth of greigite. Earth and Planetary Science Letters 277, 223–235.

Sakamoto, T., Janecek, T., Emeis, K.C., 1998. Continuous sedimentary sequences from the eastern Mediterranean Sea: composite depth sections. In: Robertson, A.H.F., Emeis, K.-C., Richter, C., Camerlenghi, A. (Eds.), Proceedings of the Ocean Drilling Program: Scientific Results, 160, pp. 37–59.

Schenau, S.J., Antonarakou, A., Hilgen, F.J., Lourens, L.J., Nijenhuis, I.A., van der Weijden, C.H., Zachariasse, W.J., 1999. Organic-rich layers in the Metochia section (Gavdos, Greece): evidence for a single mechanism of sapropel formation during the past 10 My. Marine Geology 153, 117–135.

Scrivner, A.E., Vance, D., Rohling, E.J., 2004. New neodymium isotope data quantify Nile involvement in Mediterranean anoxic episodes. Geology 32, 565–568.

Shipboard Scientific Party, 1996. Site 967. In: Emeis, K.-C., Robertson, A.H.F., Richter, C. (Eds.), Proceedings of the Ocean Drilling Program: Initial Reports, 160, pp. 215–287.

Thomson, J., Higgs, N.C., Wilson, T.R.S., Croudace, I.W., de Lange, G.J., van Santvoort, P.J.M., 1995. Redistribution and geochemical behavior of redox-sensitive elements around S1, the most recent eastern Mediterranean sapropel. Geochimica et Cosmochimica Acta 59, 3487–3501.

Thomson, J., Mercone, D., de Lange, G.J., van Santvoort, P.J.M., 1999. Review of recent advances in the interpretation of Eastern Mediterranean sapropel S1 from geochemical evidence. Marine Geology 153, 77–89.

Torrent, J., Liu, Q.S., Bloemendal, J., Barrón, V., 2007. Magnetic enhancement and iron oxides in the upper Luochuan loess–paleosol sequence, Chinese Loess Plateau. Soil Science Society of America 71, 1570–1578.

Trauth, M.H., Larrasoaña, J.C., Mudelsee, M., 2009. Trends, rhythms and events in Plio-Pleistocene African climate. Quaternary Science Reviews 28, 399–411.

Tuenter, E., Weber, S.L., Hilgen, F.J., Lourens, L.J., 2003. The response of the African summer monsoon to remote and local forcing due to precession and obliquity. Global and Planetary Change 36, 219–235.

Tzedakis, P.C., 2007. Seven ambiguities in the Mediterranean palaeoenvironmental narrative. Quaternary Science Reviews 26, 2042–2066.

Tzedakis, P.C., 2009. Cenozoic climate and vegetation change. In: Woodward, J.C. (Ed.), The Physical Geography of the Mediterranean. Oxford University Press, Oxford, pp. 89–137.

van Santvoort, P.J.M., de Lange, G.J., Langereis, C.G., Dekkers, M.J., Paterne, M., 1997. Geochemical and paleomagnetic evidence for the occurrence of "missing" sapropels in eastern Mediterranean sediments. Paleoceanography 12, 773–786.

Warning, B., Brumsack, H.-J., 2000. Trace metal signatures of eastern Mediterranean sapropels. Palaeogeography, Palaeoclimatology, Palaeoecology 158, 293–309.

Wehausen, R., Brumsack, H.-J., 2000. Chemical cycles in Pliocene sapropel-bearing and sapropel-barren eastern Mediterranean sediments. Palaeogeography, Palaeoclimatology, Palaeoecology 158, 325–352.

Weldeab, S., Emeis, K.C., Hemleben, C., Siebel, W., 2002. Provenance of lithogenic surface sediments and pathways of riverine suspended matter in the eastern Mediterranean Sea: evidence from $^{143}Nd/^{144}Nd$ and $^{87}Sr/^{86}Sr$ ratios. Chemical Geology 186, 139–149.